

## Spin and orbital magnetic moments of deposited small iron clusters studied by x-ray magnetic circular dichroism spectroscopy

This article has been downloaded from IOPscience. Please scroll down to see the full text article.

2002 New J. Phys. 4 98

(<http://iopscience.iop.org/1367-2630/4/1/398>)

View [the table of contents for this issue](#), or go to the [journal homepage](#) for more

Download details:

IP Address: 38.107.179.214

The article was downloaded on 20/02/2012 at 07:46

Please note that [terms and conditions apply](#).

## Spin and orbital magnetic moments of deposited small iron clusters studied by x-ray magnetic circular dichroism spectroscopy

J T Lau, A Föhlisch, M Martins, R Nietubycè, M Reif and W Wurth

Universität Hamburg, Institut für Experimentalphysik, Luruper Chaussee 149, D-22761 Hamburg, Germany

E-mail: [wilfried.wurth@desy.de](mailto:wilfried.wurth@desy.de)

*New Journal of Physics* 4 (2002) 98.1–98.12 (<http://www.njp.org/>)

Received 11 July 2002, in final form 14 October 2002

Published 12 December 2002

**Abstract.** The size-dependent magnetic properties of small iron clusters deposited on ultrathin Ni/Cu(100) films have been studied with circularly polarized synchrotron radiation. For x-ray magnetic circular dichroism studies, the magnetic moments of size-selected clusters were aligned perpendicular to the sample surface. Exchange coupling of the clusters to the ultrathin Ni/Cu(100) film determines the orientation of their magnetic moments. All clusters are coupled ferromagnetically to the underlayer.

With the use of sum rules, orbital and spin magnetic moments as well as their ratios have been extracted from x-ray magnetic circular dichroism spectra. The ratio of orbital to spin magnetic moments varies considerably as a function of cluster size, reflecting the dependence of magnetic properties on cluster size and geometry. These variations can be explained in terms of a strongly size-dependent orbital moment. Both orbital and spin magnetic moments are significantly enhanced in small clusters as compared to bulk iron, although this effect is more pronounced for the orbital moment.

Magnetic properties of deposited clusters are governed by the interplay of cluster-specific properties on the one hand and cluster–substrate interactions on the other hand. Size dependent variations of magnetic moments are modified upon contact with the substrate.

## 1. Introduction

Clusters are fascinating objects because of their unique physical properties which are intricately linked to the cluster size. This holds for a variety of chemical, optical and magnetic properties that are governed by the specific electronic structure of a cluster. With regard to magnetism, small transition metal clusters are well suited to study the evolution from the localized magnetic moments that characterize all atoms with open shells to the itinerant magnetism in the ferromagnetic 3d transition metals iron, cobalt and nickel. In the case of iron, for instance, the magnetic moment is reduced from  $6 \mu_B$  for the free atom to  $2.2 \mu_B$  in the bulk.

In free cluster beams, the magnetic moments of size selected transition metal clusters have been studied in Stern–Gerlach experiments [1]–[4], investigating the average magnetic moment per atom down to cluster sizes of only a few atoms per cluster. For the ferromagnetic 3d transition metals, these experiments have shown that the clusters approach bulk magnetic moments already for cluster sizes of only a few hundred atoms per cluster [2, 3]. This approach to bulk magnetism, however, does not occur smoothly with increasing cluster size, but characteristic shell effects are observed. For very small clusters consisting of only a few atoms [4], the average magnetic moment can vary drastically upon changing the cluster size by just one atom.

Magnetism of transition metal clusters is interesting not only from the point of view of their fundamental physical properties, but also for potential applications in magnetic data storage or magnetoelectronic devices. For application, however, magnetic clusters have to be supported on a substrate. This can substantially alter their properties because of electronic interaction of the clusters with the substrate, or because of geometric rearrangement of the cluster atoms. A detailed understanding of magnetism on a nanoscale in either free or supported clusters can only be achieved by carefully studying size selected clusters in experimental conditions where well defined cluster samples can be prepared. For cluster deposition in particular, fragmentation as well as agglomeration of the clusters on the substrate needs to be avoided. Furthermore, ultra-high vacuum (UHV) conditions are essential to rule out adsorption of residual gas molecules on the clusters.

## 2. Experimental set-up and technique

To investigate magnetic moments of small transition metal clusters, we have set up a cluster source that allows us to deposit truly size-selected clusters onto single crystal substrates under soft landing conditions in UHV.

Small iron clusters are produced with a sputter source by bombardment of a high purity (99.95%) iron sputter target with 28 keV  $\text{Xe}^+$  ions. Positively charged iron clusters are accelerated to 500 eV and a cluster beam is formed. For mass separation, a magnetic dipole field is used. Depending on the specific element used, mass-separated cluster current densities are on the order of  $50 \text{ pA mm}^{-2}$  to  $5 \text{ nA mm}^{-2}$  for cluster ions of 1–10 atoms per cluster. In figure 1 this is illustrated for the case of  $\text{Fe}_n^+$  cluster ions. Soft landing [5]–[8] of the clusters is achieved by deceleration of the cluster ion beam to a kinetic energy of less than 1–2 eV per atom as well as by cluster deposition into argon multilayers. The coverage of cluster atoms on the surface is less than 0.03 monolayers to avoid cluster agglomeration. For the same reason, all experiments are carried out at temperatures of less than 20 K. A detailed description of the experimental set-up is given in [9]–[12].

To study the magnetic moments of deposited iron clusters, an ultrathin Ni/Cu(100) film is

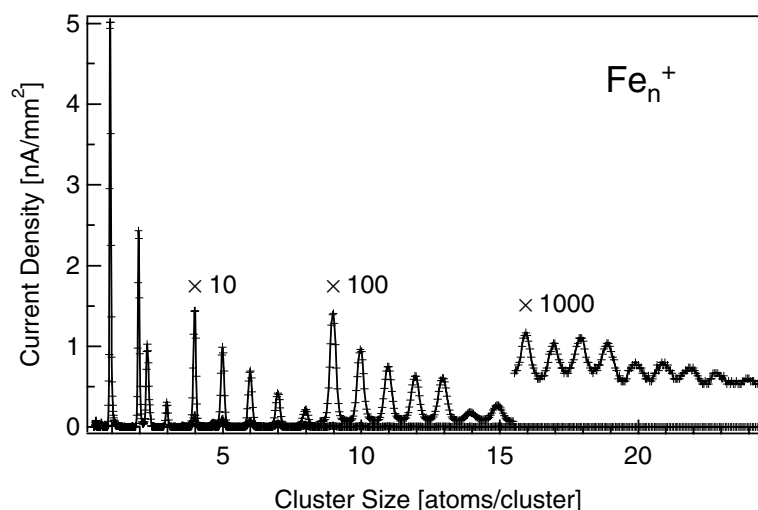


**Figure 1.** Mass spectrum of small iron clusters. Cluster current densities are measured at the sample position.

chosen as the substrate for cluster deposition. The nickel film thickness is monitored *in situ* by x-ray absorption spectroscopy at the nickel and copper  $L_3$  edges, and ranges approximately from 20 to 40 monolayers. Because of their perpendicular magnetic anisotropy [13]–[15], these films can be magnetized to remanence perpendicular to the film surface. Exchange coupling of the deposited iron clusters to the Ni/Cu(100) underlayer aligns their magnetic moments parallel to the surface normal as can be shown experimentally [12, 11]. By studying clusters on a thin magnetic substrate, their magnetic moments can be aligned without the presence of strong magnetic fields in the experimental chamber.

*In situ* sample preparation is carried out in UHV conditions. A Cu(100) single crystal is cleaned by repeated cycles of sputtering with 1500 eV  $\text{Ar}^+$  ions and annealing at 900 K. Ultrathin nickel films are prepared by evaporation from a high purity (99.999%) nickel foil in UHV at growth rates of 2–4 ML  $\text{min}^{-1}$  at a pressure of  $\leq 5 \times 10^{-10}$  mbar, followed by annealing at 400 K. The nickel films are magnetized by applying a magnetic field of  $\geq 100$  mT perpendicular to the sample surface with a solenoid. Prior to cluster deposition, the Ni/Cu(100) substrate is covered with approximately 20 layers of argon for soft landing. After cluster deposition, the argon buffer layers are desorbed by heating the sample to 100 K, leaving the iron clusters on the bare Ni/Cu(100) surface. The magnetic properties of small size-selected iron clusters on an Ni/Cu(100) underlayer have been studied by measuring their x-ray magnetic circular dichroism (XMCD) in core level x-ray absorption. XMCD is a valuable technique to determine magnetic spin and orbital moments separately [16]–[19]. Since it is based on resonant x-ray absorption spectroscopy, XMCD is an element specific and highly sensitive probe and is ideally suited to study dilute heterogeneous samples such as a submonolayer coverage of size-selected clusters on a substrate.

The magnetic moments of itinerant 3d metals are probed by core level x-ray absorption with electron transitions from 2p to 3d levels. Excitation at the spin–orbit split  $2p_{3/2}$  ( $L_3$  edge) and  $2p_{1/2}$  ( $L_2$  edge) levels with circularly polarized synchrotron light yields transitions of spin polarized electrons due to the Fano effect [20]. With these spin polarized electrons, the exchange split unoccupied density of states above the Fermi level of a magnetized sample can be probed,

giving information about the magnetic spin moment. Simultaneously, because of the angular momentum transfer from the circularly polarized x-ray photons to the orbital angular momentum of the electrons, the orbital magnetic moment of the 3d states can be probed.

XMCD sum rules [17]–[19] link the difference in x-ray absorption cross sections of a magnetized sample for left- and right-handed circular polarization to the expectation values of  $S_z$  and  $L_z$ . For 2p–3d transitions, these sum rules are

$$\langle L_z \rangle = 2n_h \frac{\int_{L_3+L_2} \sigma^+ - \sigma^- dE}{\int_{L_3+L_2} \sigma^+ + \sigma^0 + \sigma^- dE}$$

for the expectation value of the orbital angular momentum  $\langle L_z \rangle$  and

$$\langle S_z \rangle + \frac{7}{2} \langle T_z \rangle = \frac{3}{2} n_h \frac{\int_{L_3} \sigma^+ - \sigma^- dE - 2 \int_{L_2} \sigma^+ - \sigma^- dE}{\int_{L_3+L_2} \sigma^+ + \sigma^0 + \sigma^- dE}$$

for the expectation value of the spin angular momentum  $\langle S_z \rangle$  and the expectation value of the magnetic dipole operator  $\langle T_z \rangle$ , which is a measure of the anisotropy of the spin distribution within the atomic volume. The term  $(\mu_B/\hbar)\langle T_z \rangle$  is also known as the magnetic dipole contribution or dipole term  $m_T$ . In these XMCD sum rules,  $n_h$  is the number of unoccupied 3d states,  $\sigma^+$  and  $\sigma^-$  are absorption coefficients measured with parallel and antiparallel orientation of sample magnetization  $\vec{M}$  and photon helicity  $\vec{\sigma}$ , respectively, and  $\sigma^0$  is the absorption coefficient measured with linearly polarized soft x-rays and parallel orientation of sample magnetization  $\vec{M}$  and photon polarization  $\vec{E}$ . The XMCD asymmetry  $\sigma^+ - \sigma^-$  is a measure of spin imbalance in the valence states, and  $L_2$  and  $L_3$  denote the limits of integration at the  $L_2$  and  $L_3$  edges of the x-ray absorption spectra. The validity of these sum rules has been shown experimentally for bulk 3d metals [21].

XMCD spectra of deposited iron clusters on Ni/Cu(100) were taken at BESSY II elliptically undulator beamline UE56/1-PGM [22] in normal incidence geometry with a photon polarization of 90% and energy resolution of 280 meV at the iron  $L_{2,3}$  edges. X-ray absorption of the clusters was recorded in partial and total electron yield detection mode. XMCD spectra were cross checked for systematic errors by switching sample magnetization and photon helicity.

### 3. Results and discussion

By a simple comparison of the XMCD asymmetries at the iron and nickel  $L_{2,3}$  edges, the coupling of the deposited iron clusters to the Ni/Cu(100) substrate can be determined. As shown in figure 2 for  $\text{Fe}_7$  as an example representative for the behaviour of all deposited iron clusters studied, the iron and nickel asymmetries have the same sign at their respective  $L_3$  and  $L_2$  edges, and therefore possess the same kind of majority spin carriers. From this it can be inferred that all deposited iron clusters are coupled ferromagnetically to the Ni/Cu(100) substrate.

This result is in line with studies of ultrathin iron films on Ni/Cu(100) [23, 24]. For these systems, it has been shown that the magnetization of an ultrathin iron film always follows the direction of magnetization of the Ni/Cu(100) substrate [23, 24]. Ferromagnetic coupling of iron adatoms to Ni(100) is also expected from theoretical predictions [25]. Exchange coupling of the iron clusters to the saturated Ni/Cu(100) substrate also provides saturation magnetization for the iron clusters.

The use of XMCD sum rules to extract spin and orbital magnetic moments relies on the knowledge of the number  $n_h$  of unoccupied 3d states and on proper normalization of the XMCD

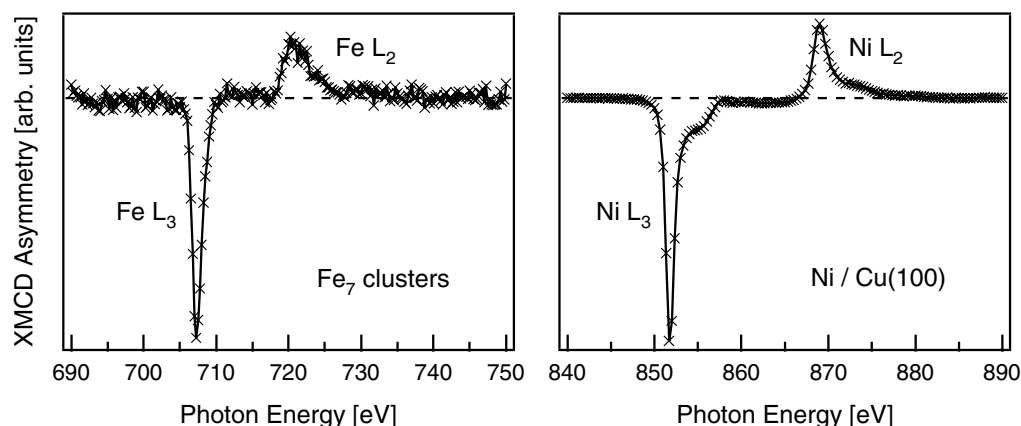


**Figure 2.** XMCD asymmetries of deposited iron clusters (left) and the Ni/Cu(100) substrate (right). All iron clusters are coupled ferromagnetically to the substrate.

asymmetry. Unfortunately, the exact number of unoccupied 3d states per atom is not known for small iron clusters on Ni/Cu(100). Furthermore, the exact normalization of the XMCD asymmetry to the total number of unoccupied 3d states probed in the x-ray absorption experiment is not a trivial task. Both  $n_h$  and the normalization will introduce a certain error when applying the XMCD sum rules. However, the ratio of orbital to spin magnetic moment can be determined from the XMCD asymmetry with only little uncertainty according to

$$\frac{m_l}{m_s} = \frac{2 \int_{L_3} \sigma^+ - \sigma^- dE + \int_{L_2} \sigma^+ - \sigma^- dE}{3 \int_{L_3} \sigma^+ - \sigma^- dE - 2 \int_{L_2} \sigma^+ - \sigma^- dE}.$$

Clearly, this ratio does not depend on  $n_h$  or on any normalization of the XMCD asymmetry  $\sigma^+ - \sigma^-$ .

In figure 3 the ratios of orbital to spin magnetic moments are given for  $\text{Fe}_2$ – $\text{Fe}_9$  on Ni/Cu(100). This ratio is considerably larger than the ratio for bulk iron [21], ultrathin iron films [26]–[30] or iron nanoclusters [31] with a mean cluster size of roughly 400 atoms per cluster. This is an indication of an increase in orbital magnetism with reduction in dimensionality. Furthermore, strong size-specific variations in the ratio of  $m_l$  to  $m_s$  can be seen in figure 3. This is a hint at a strong dependence of orbital or spin magnetic moments on the exact number of atoms per cluster [12].

To attribute this variation to changes in  $m_l$ ,  $m_s$  or both, spin and orbital magnetic moments per unoccupied 3d state have to be evaluated. To extract these values from the iron clusters' XMCD asymmetries, the measured XMCD asymmetry has to be normalized to the total number of unoccupied 3d states participating in x-ray absorption, which is proportional to  $\sigma^+ + \sigma^0 + \sigma^-$ . In our analysis, we assumed  $\sigma^0$  to be equal to  $1/2(\sigma^+ + \sigma^-)$ , although this assumption is likely to fail for highly anisotropic systems such as small clusters on a substrate [32, 33]. In addition, the XMCD asymmetry needs to be corrected for incomplete photon polarization, not fully saturated sample magnetization, and possible deviation from a parallel alignment of photon helicity and sample magnetization.

Since the magnetization of the Ni/Cu(100) underlayer was monitored by XMCD at the nickel  $L_{2,3}$  edges for each cluster sample, and since all  $\text{Fe}_n$  clusters are coupled ferromagnetically to the substrate, the magnetization of the Ni/Cu(100) substrate can be used as a measure of sample

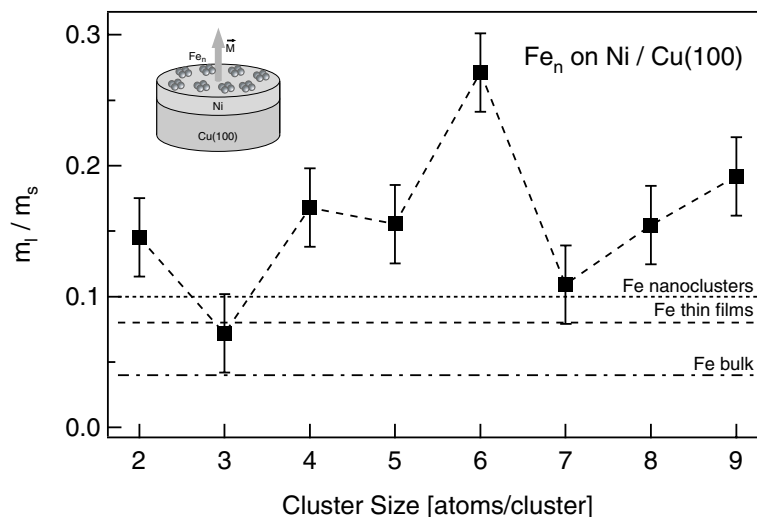


**Figure 3.** Ratio of orbital to spin magnetic moments for small iron clusters on Ni/Cu(100) as shown in the inset, compared to bulk iron [21], thin iron films [26]–[30] and supported iron nanoclusters [31]. The inset schematically shows a sample of size selected iron clusters on Ni/Cu(100).

magnetization and alignment [11]. The procedure is illustrated in figure 4. Here, the out-of-plane component of the Ni/Cu(100) magnetic spin moment is compared to the out-of-plane magnetic spin moment of the iron clusters before normalization. The observed variation of the out-of-plane magnetic remanence of the Ni/Cu(100) substrate can be correlated with the nickel film thickness [11] and might be due to the spin reorientation transition from out-of-plane to in-plane orientation [34]–[40]. Within an experimental error of 10%, the ultrathin Ni/Cu(100) films which were prepared as substrates for Fe<sub>4</sub>–Fe<sub>8</sub> carry the same magnetic spin moment per unoccupied 3d state. This is the case of out-of-plane saturation magnetization of the Ni/Cu(100) substrate. For Fe<sub>2</sub>, Fe<sub>3</sub> and Fe<sub>9</sub>, however, Ni/Cu(100) films were prepared with a film thickness where the spin reorientation transition from out-of-plane to in-plane magnetization has already begun [37]–[40]. The resulting average magnetization of the macroscopic sample area probed by the synchrotron radiation beam will therefore no longer be saturated perpendicular to the ultrathin Ni/Cu(100) film. As a result, the measured out-of-plane component of magnetization of these Ni/Cu(100) films is lower than expected. Because of the ferromagnetic coupling of the iron clusters to the ultrathin nickel film, the measured (average) out-of-plane magnetization of the iron clusters follows the (average) magnetization direction of the Ni/Cu(100) substrate, and will be lower as well. In addition, slight deviations from a parallel alignment of photon helicity and sample magnetization could also lower the observed magnetic moment. To compensate for this, the cluster magnetic moments have been normalized to the out-of-plane magnetic moment of their respective Ni/Cu(100) substrate, with the dotted line in figure 4 used as a reference. This improved normalization procedure, taking into account subtle differences in sample magnetization [11], results in magnetic spin and orbital moments that are up to 15% larger than those reported previously [12].

In figure 5, the magnetic spin moments per unoccupied 3d state are given for Fe<sub>2</sub>–Fe<sub>9</sub> on Ni/Cu(100). These values are corrected for photon polarization and sample magnetization as described above. The error bars in figure 5 are a conservative estimate of the experimental

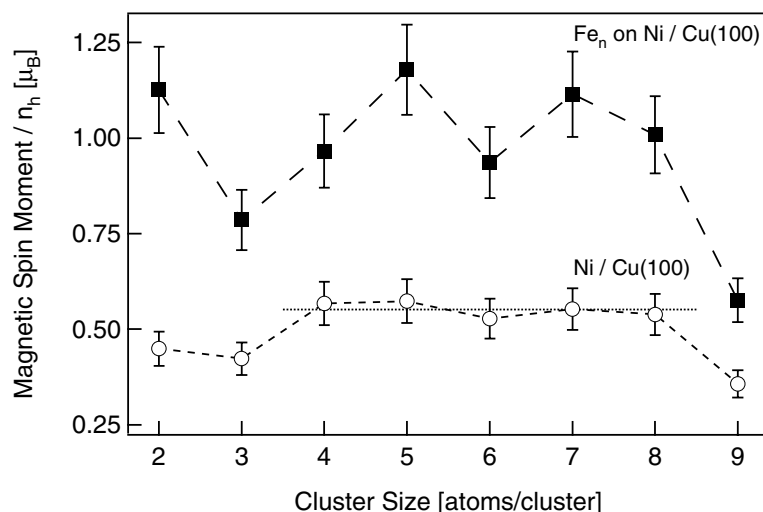


**Figure 4.** Magnetic spin moments per unoccupied 3d state for deposited iron clusters and the respective Ni/Cu(100) substrate. Not fully saturated perpendicular magnetization of the substrate leads to reduced magnetic moments for Fe<sub>2</sub>, Fe<sub>3</sub> and Fe<sub>9</sub>, and has to be corrected for.

uncertainty. As can be seen, the magnetic spin moments are enhanced for all iron clusters as compared to the bulk value of  $0.65 \mu_B$  per unoccupied 3d state. For Fe<sub>3</sub>–Fe<sub>9</sub>, the spin moment is roughly constant and varies around  $1 \mu_B$  per unoccupied 3d state. Fe<sub>2</sub> has a much larger spin moment of about  $1.3$ – $1.4 \mu_B$  per unoccupied 3d state. Since the isotropic spin moment per 3d hole cannot exceed  $1 \mu_B$ , the additional contribution is attributed to  $7 m_T$ , which in most cases cannot be separated from  $m_s$  in the spin sum rule. Only for isotropic systems can  $7 m_T$  be neglected, as is the case for bulk metals [21, 41]. The largest contribution of  $7 m_T$  to the spin sum rule is found for Fe<sub>2</sub>, the smallest cluster studied. The biggest cluster in the series, Fe<sub>9</sub>, shows the lowest value of  $m_s + 7 m_T$ . In general, one would expect a decrease of  $m_s + 7 m_T$  with increasing cluster size.

The orbital magnetic moments per unoccupied 3d state of the deposited iron clusters are shown in figure 6. Again, the values are normalized as discussed above. Large error bars are deliberately chosen to give a conservative estimate of  $m_l$ . As compared to bulk iron, where the orbital moment of only  $0.04 \mu_B$  is quenched by the crystal field, the orbital moment of the clusters is even more enhanced than the spin moment. Furthermore, the orbital magnetic moment in figure 6 shows a strong non-monotonic variation with cluster size. This variation is very similar to the one found for the ratio of orbital to spin magnetic moments shown in figure 3. The variation in the ratio of orbital to spin moment can therefore almost exclusively be attributed to the variation in orbital magnetic moment, although at this stage, the reason for this strong dependence still has to be investigated experimentally or theoretically.

To compare spin and orbital magnetic moments of deposited iron clusters on Ni/Cu(100) to those of free cluster beams [2]–[4] or theoretical values [42]–[45] for deposited iron clusters, the magnetic moments have to be given as per atom values. Therefore, to fully apply the XMCD sum rules,  $n_h$  needs to be known and  $m_s$  has to be separated from  $7 m_T$  in the spin sum rule. For this, the number  $n_h$  of unoccupied 3d states for small iron clusters on Ni/Cu(100) was estimated to be in the range of  $3.39$ – $3.66$  per atom, which is in between theoretical values for bulk bcc iron,

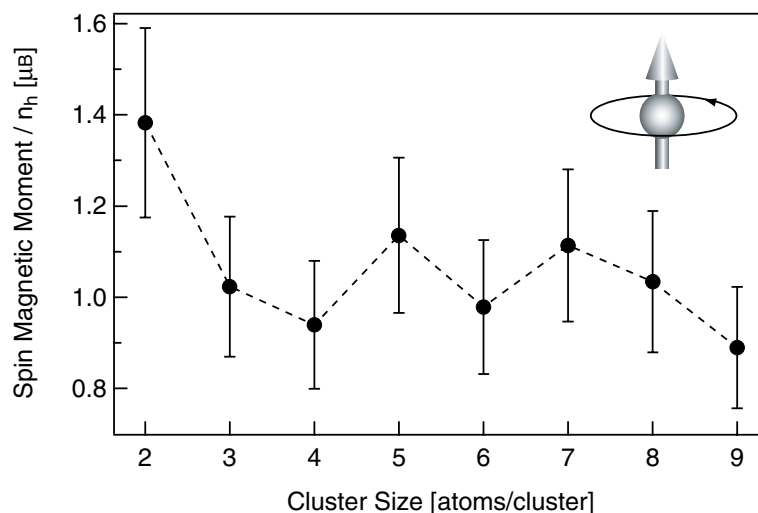


**Figure 5.** Normalized spin magnetic moments  $m_s + 7m_T$  per unoccupied 3d state for deposited iron clusters on a Ni/Cu(100) substrate. The magnetic moments shown here are up to 15% larger than those reported previously [12].

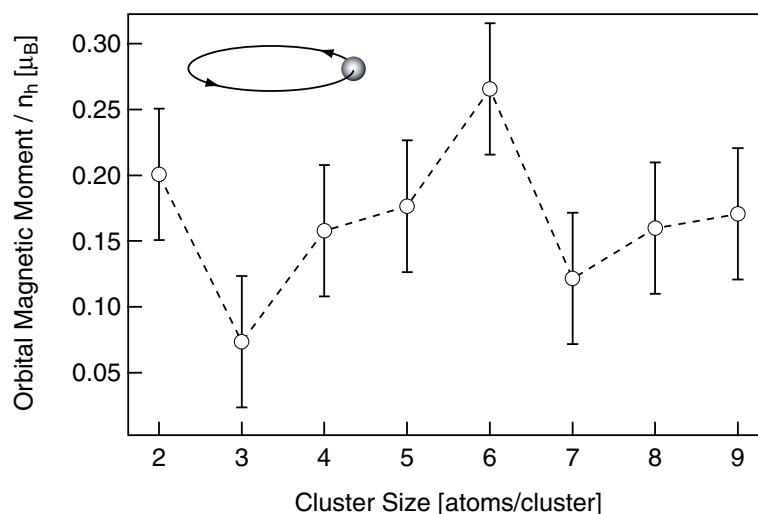


**Figure 6.** Normalized magnetic orbital moments per unoccupied 3d state for deposited iron clusters on a Ni/Cu(100) substrate. The magnetic moments shown here are up to 15% larger than those reported previously [12] (cf figure 3).

bulk fcc iron [46] and a NiFe<sub>3</sub> alloy [47]. The number of unoccupied 3d states is not expected to vary strongly with cluster size [48].

To apply the spin sum rule to the experimental data, the magnetic dipole contribution  $7m_T$  to the spin magnetic moment was estimated to be 25–35% of  $m_s$ , which is the value of  $7m_T$  that is expected at surfaces of the 3d metals [49]. For Fe<sub>2</sub> with an obviously larger contribution of the magnetic dipole term, however,  $7m_T$  was estimated to be 40–50% of  $m_s$ . Unfortunately, these estimates necessary for comparison of the data will introduce an additional error in the absolute values of  $m_s$  and  $m_l$ .

**Table 1.** Measured spin and orbital magnetic moments of small iron clusters on Ni/Cu(100) before and after normalization. Also given are rough estimates of the per atom values of the magnetic moments.

	Fe <sub>2</sub>	Fe <sub>3</sub>	Fe <sub>4</sub>	Fe <sub>5</sub>	Fe <sub>6</sub>	Fe <sub>7</sub>	Fe <sub>8</sub>	Fe <sub>9</sub>
$(m_s + 7 m_T)/n_h (\mu_B)$								
raw	1.13	0.79	0.97	1.18	0.94	1.11	1.01	0.58
normalized	1.38	1.02	0.94	1.14	0.98	1.11	1.03	0.89
$m_l/n_h (\mu_B)$								
raw	0.16	0.06	0.16	0.18	0.25	0.12	0.16	0.11
normalized	0.20	0.07	0.16	0.18	0.27	0.12	0.16	0.17
$(m_s + 7 m_T + m_l)/n_h (\mu_B)$								
raw	1.29	0.84	1.13	1.36	1.19	1.24	1.16	0.69
normalized	1.58	1.10	1.10	1.31	1.24	1.24	1.19	1.06
$m_l/(m_s + 7 m_T)$	0.15	0.07	0.17	0.16	0.27	0.11	0.15	0.19
$m_s$ per atom ( $\mu_B$ )								
( $\pm 0.6 \mu_B$ )	3.3	2.5	2.3	3.0	2.4	2.9	2.6	2.1
$m_l$ per atom ( $\mu_B$ )								
( $\pm 0.15 \mu_B$ )	0.71	0.26	0.56	0.63	0.94	0.43	0.57	0.60
$m_s + m_l$ per atom ( $\mu_B$ )								
( $\pm 0.7 \mu_B$ )	4.0	2.8	2.9	3.6	3.4	3.3	3.2	2.7

The spin magnetic moments per atom for small iron clusters on Ni/Cu(100) are approximately 2.3–3  $\mu_B$  for Fe<sub>3</sub>–Fe<sub>8</sub>, 2.1  $\mu_B$  for Fe<sub>9</sub> and 3.3  $\mu_B$  for Fe<sub>2</sub>. Orbital magnetic moments are 0.6  $\mu_B$  for Fe<sub>2</sub>, Fe<sub>4</sub>, Fe<sub>5</sub>, Fe<sub>8</sub> and Fe<sub>9</sub>. For Fe<sub>3</sub>, the orbital magnetic moment is 0.3  $\mu_B$  and for Fe<sub>6</sub> it is 0.9  $\mu_B$ . The total magnetic moment is 2.8–3.6  $\mu_B$  per atom for Fe<sub>3</sub>–Fe<sub>8</sub>, 2.7  $\mu_B$  for Fe<sub>9</sub> and 4.0  $\mu_B$  per atom for Fe<sub>2</sub>. These magnetic moments are summarized in table 1 and compared to the moments per unoccupied 3d state before and after normalization. The magnetic spin and orbital moments per atom are enhanced for all clusters as compared to bulk iron, although the effect is clearly more pronounced for the orbital moment.

For iron cluster beams in Stern–Gerlach experiments, the total magnetic moment is 4–6  $\mu_B$  per atom for Fe<sub>10</sub> through Fe<sub>12</sub> [4]. Compared to these free cluster values, the magnetic moments of small iron clusters are reduced after deposition. A possible explanation could be an increase in the average coordination number of the cluster atoms on the surface. In two-dimensional clusters on the Ni/Cu(100) fcc surface, even the least coordinated cluster atoms have four nearest neighbours in the nickel substrate. Furthermore, the structures and bond lengths of deposited clusters will deviate from those of free clusters. Also, electronic interaction and hybridization of the iron and nickel 3d electrons could result in a reduction of the magnetic moments as compared to those of free clusters [2]–[4].

Although theoretical predictions for magnetic moments of small iron clusters on a Ni(100) surface are not available yet to the best of our knowledge, the experimental results can be compared to calculated magnetic moments for small iron clusters on Ag(100) [42]–[45]. These calculations, assuming two-dimensional cluster structures such as those shown in figure 7, predict a spin moment of 3.2–3.3  $\mu_B$  per atom that shows only very little dependence on cluster size. This theoretical result corroborates our experimental findings for the spin moment of small iron

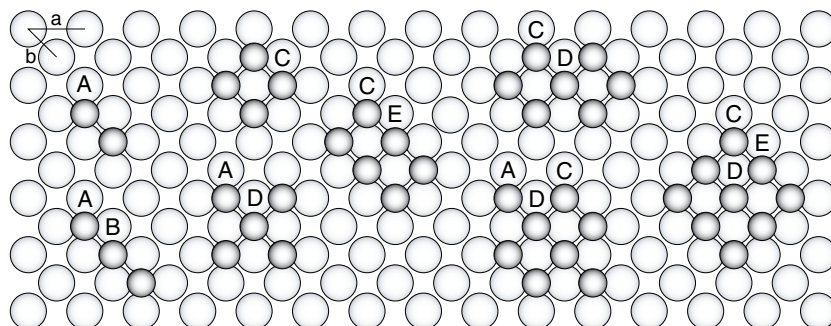


**Figure 7.** Possible two-dimensional pseudomorphic arrangements of small iron clusters on fcc Ni/Cu(100) [42]–[45]. The lattice parameter  $a$  and the nearest neighbour distance  $b$  are different for Ag(100) and Ni/Cu(100) substrates.

clusters on Ni/Cu(100) in figure 5. Here, with the exception of  $\text{Fe}_2$ , the spin magnetic moments also depends only weakly on cluster size.

On the other hand, the predicted spin magnetic moments for iron adclusters on Ag(100) are generally larger than those found experimentally for iron clusters on Ni/Cu(100). This discrepancy could be explained in terms of different lattice constants of fcc silver and fcc nickel. Given that the iron cluster atoms will occupy fcc lattice sites on the fcc substrate, the nearest neighbour distance within the iron adcluster on Ag(100) will be  $2.89 \text{ \AA}$ , whereas on Ni/Cu(100) it is only  $2.49 \text{ \AA}$ . Because of an increased overlap of iron 3d electrons, a decrease in nearest-neighbour distance will result in a decrease of magnetic moments. Also, the electronic interaction of iron clusters with the Ni/Cu(100) substrate will be different from a Ag(100) substrate due to differences in 3d level occupation. Thus it is not surprising that iron clusters on Ag(100) should carry larger moments than iron clusters on Ni/Cu(100).

In table 2, theoretical spin and orbital magnetic moments [42, 43] are compared for different coordination numbers. For the orbital magnetic moment, the predictions for iron clusters on Ag(100) show a much stronger dependence on cluster size [42]–[45] than for the spin moment. This is also what is found experimentally for iron clusters on Ni/Cu(100), although the experimental values for iron clusters on Ni/Cu(100) show a much stronger variation with cluster size than calculated orbital moments for iron clusters on Ag(100). However, the calculated average orbital moments of  $0.2\text{--}0.4 \mu_B$  per atom are smaller than those determined experimentally. This might be due to the difficulty in calculating orbital moments with high precision. Further theoretical work will hopefully illuminate the physics behind the strong variation in orbital magnetic moments of iron clusters on Ni/Cu(100).

#### 4. Summary

The magnetic spin and orbital moments were measured by XMCD in 2p–3d x-ray absorption for small, mass selected iron clusters on Ni/Cu(100) in the size range from  $\text{Fe}_2$  to  $\text{Fe}_9$ . All clusters are coupled ferromagnetically to the magnetized substrate. Already in the ratio of spin to orbital magnetic moments a strong dependence of cluster magnetism on cluster size is found. This can almost exclusively be attributed to a variation in orbital magnetic moments with cluster size, whereas the spin magnetic moment is roughly constant for  $\text{Fe}_3\text{--}\text{Fe}_9$ . Only  $\text{Fe}_2$  shows a much

**Table 2.** Calculated spin and orbital magnetic moments of small fcc iron clusters on Ag(100) [42, 43]. Labelling of iron cluster atoms A–D according to figure 7.

Atom number	Coordination number	Orbital moment ( $\mu_B$ )				Spin moment ( $\mu_B$ )			
		Fe <sub>2</sub>	Fe <sub>3</sub>	Fe <sub>4</sub>	Fe <sub>5</sub>	Fe <sub>2</sub>	Fe <sub>3</sub>	Fe <sub>4</sub>	Fe <sub>5</sub>
A [42]	1	0.28	0.35		0.32	3.20	3.26		3.29
		0.32	0.44		0.37	3.31	3.33		3.35
B [42]	2		0.22				3.26		
			0.25				3.33		
C [42]	2			0.20					3.21
				0.18					3.26
D [42]	4				0.14				3.10
					0.12				3.15
Average [42]		0.28	0.30	0.20	0.28	3.28	3.26	3.21	3.25
Average [43]		0.32	0.38	0.18	0.33	3.31	3.32	3.26	3.21

larger spin moment than the other clusters. In general, all clusters possess enhanced spin and orbital magnetic moments as compared to bulk iron, although their moments are smaller than would be expected for free clusters. This effect is even more pronounced for the orbital moments than for the spin moments. Calculations for iron adclusters on Ag(100) also predict enhanced magnetic moments, and a stronger variation is expected for the orbital than for the spin moment. This is due to the higher sensitivity of the orbital moment to changes in coordination number, as given by theory.

In the future, joint experimental and theoretical efforts will hopefully elucidate the physical explanation for the behaviour of small iron clusters on Ni/Cu(100).

## Acknowledgments

We acknowledge technical support by BESSY staff members F Senf, G Reichard and M Mast. This project was funded by BMBF through grant KS1GUB/5.

## References

- [1] Cox D M, Trevor D J, Whetten R L, Rohlfing E A and Kaldor A 1985 *Phys. Rev. B* **32** 7290
- [2] Billas I M L, Becker J A, Châtelain A and de Heer W A 1993 *Phys. Rev. Lett.* **71** 4067
- [3] Billas I M L, Châtelain A and de Heer W A 1994 *Science* **265** 1682
- [4] Knickelbein M B 2002 *Chem. Phys. Lett.* **353** 221
- [5] Cheng H-P and Landman U 1993 *Science* **260** 1304
- [6] Cheng H-P and Landman U 1994 *J. Phys. Chem.* **98** 3527
- [7] Bromann K, Félix C, Brune H, Harbich W, Monot R, Buttet J and Kern K 1996 *Science* **274** 956
- [8] Bromann K, Brune H, Félix C, Harbich W, Monot R, Buttet J and Kern K 1997 *Surf. Sci.* **377–379** 1051
- [9] Lau J T, Achleitner A and Wurth W 2000 *Chem. Phys. Lett.* **317** 269
- [10] Lau J T, Achleitner A and Wurth W 2000 *Surf. Sci.* **467** 834

- [11] Lau J T 2002 *PhD Thesis* Universität Hamburg DESY-THESIS-2002-016
- [12] Lau J T, Föhlisch A, Nietubyc R, Reif M and Wurth W 2002 *Phys. Rev. Lett.* **89** 057201
- [13] O'Brien W L and Tonner B P 1994 *Phys. Rev. B* **49** 15370
- [14] Schulz B and Baberschke K 1994 *Phys. Rev. B* **50** 13467
- [15] Le Fèvre P, Magnan H and Chandesris D 1999 *Eur. Phys. J. B* **10** 555
- [16] Thole B, Carra P and van der Laan G 1992 *Phys. Rev. Lett.* **68** 1943
- [17] Altarelli M 1993 *Phys. Rev. B* **47** 597
- [18] Carra P, Thole B T, Altarelli M and Wang X 1993 *Phys. Rev. Lett.* **70** 694
- [19] van der Laan G 1998 *Phys. Rev. B* **57** 112
- [20] Fano U 1969 *Phys. Rev.* **178** 131
- [21] Chen C T, Idzerda Y U, Lin H-J, Smith N V, Meigs G, Chaban E, Ho G H, Pellegrin E and Sette F 1995 *Phys. Rev. Lett.* **75** 152
- [22] Weiss M R, Follath R, Sawhney K J S, Senf F, Bahrtdt J, Frentrup W, Gaupp A, Sasaki S, Scheer M, Mertins H-C, Abramson D, Schäfers F, Kuch W and Mahler W 2001 *Nucl. Instrum. Methods A* **467/468** 449
- [23] Schirmer B and Wuttig M 1999 *Phys. Rev. B* **60** 12945
- [24] O'Brien W L and Tonner B P 1996 *J. Appl. Phys.* **79** 5629
- [25] Nonas B, Wildberger K, Zeller R and Dederichs P H 1997 *J. Magn. Magn. Mater.* **165** 137
- [26] O'Brien W L and Tonner B P 1995 *Surf. Sci.* **334** 10
- [27] Dávila M E, Arvanitis D, Hunter Dunn J, Mårtensson N, Srivastava P, Wilhelm F and Baberschke K 1999 *J. Magn. Magn. Mater.* **196/197** 120
- [28] Waddill G D and Tobin J G 1993 *J. Appl. Phys.* **73** 6748
- [29] Hunter Dunn J, Arvanitis D and Mårtensson N 1996 *Phys. Rev. B* **54** 11157
- [30] Ohresser P, Ghiringhelli G, Tjerneberg O, Brookes N B and Finazzi M 2000 *Phys. Rev. B* **62** 5803
- [31] Edmonds K W, Binns C, Baker S H, Thornton S C, Norris C, Goedkopp J B, Finazzi M and Brookes N 1999 *Phys. Rev. B* **60** 472
- [32] Stöhr J 1999 *J. Magn. Magn. Mater.* **200** 470
- [33] Daalderop G H O, Kelly P J and Schuurmans M F H 1994 *Phys. Rev. B* **50** 9989
- [34] Millev Y T, Oepen H P and Kirschner J 1998 *Phys. Rev. B* **57** 5837
- [35] Millev Y T, Oepen H P and Kirschner J 1998 *Phys. Rev. B* **57** 5848
- [36] O'Brien W L and Tonner B P 1996 *J. Appl. Phys.* **79** 5623
- [37] Uiberacker C, Zabloudil J, Weinberger P, Szunyogh L and Sommers C 1999 *Phys. Rev. Lett.* **82** 1289
- [38] Farle M, Mirwald-Schulz B, Anisimov A N, Platow W and Baberschke K 1997 *Phys. Rev. B* **55** 3708
- [39] O'Brien W L, Droubay T and Tonner B P 1996 *Phys. Rev. B* **54** 9297
- [40] Bochi G, Ballentine C A, Inglefield H E, Thomson C V, O'Handley R C, Hug H J, Stiefel B, Moser A and Güntherodt H-J 1995 *Phys. Rev. B* **52** 7311
- [41] Stöhr J 1995 *J. Electron Spectrosc. Relat. Phenom.* **75** 253
- [42] Cabria I, Nonas B, Zeller R and Dederichs P H 2002 *Phys. Rev. B* **65** 054414
- [43] Lazarovits B, Szunyogh L and Weinberger P 2002 *Phys. Rev. B* **65** 104441
- [44] Izquierdo J, Vega A, Balbás L C, Sánchez-Portal D, Junquera J, Artacho E, Soler J M and Ordejón P 2000 *Phys. Rev. B* **61** 13639
- [45] Stepanyuk V S, Hergert W, Rennert P, Wildberger K, Zeller R and Dederichs P H 1999 *Phys. Rev. B* **59** 1681
- [46] James P, Eriksson O, Johansson B and Abrikosov I A 1999 *Phys. Rev. B* **59** 419
- [47] Nautiyal T and Auluck S 1993 *Phys. Rev. B* **47** 1726
- [48] Vega A, Dorantes-Dávila J, Balbás L C and Pastor G M 1993 *Phys. Rev. B* **47** 4742
- [49] Wu R and Freeman A J 1994 *Phys. Rev. Lett.* **73** 1994